

# Improved Model Predictability by Machine Data in Computational Lithography and Application to Laser Bandwidth Tuning

Stefan Hunsche<sup>a\*</sup>, Qian Zhao<sup>a</sup>, Xu Xie<sup>a</sup>, Robert Socha<sup>b</sup>, Hua-Yu Liu<sup>a</sup>, Peter Nikolsky<sup>c</sup>, Anthony Ngai<sup>c</sup>, Paul van Adrichem<sup>c</sup>, Michael Crouse<sup>d</sup>, Ivan Lalovic<sup>e</sup>

<sup>a</sup>Brion Technologies, an ASML company, 4211 Burton Dr. Santa Clara, CA 95054;

<sup>b</sup>ASML, 4211 Burton Dr. Santa Clara, CA 95054;

<sup>c</sup>ASML Netherlands B.V., De Run 6501, 5504DR Veldhoven The Netherlands;

<sup>d</sup>ASML Corporation, 25 Corporate Circle, Albany NY 12203;

<sup>e</sup>Cymer, Inc., 17075 Thornmint Court, San Diego, CA 92127

Computational lithography (CL) is becoming more and more of a fundamental enabler of advanced semiconductor processing technology, and new requirements for CL models are arising from new applications such as model-based process tuning. In this paper we study the impact of realistic machine parameters that can be incorporated in a modern CL model, and provide an experimental assessment of model improvements with respect to prediction of scanner tuning effects. The data demonstrates improved model accuracy and prediction by inclusion of scanner-type specific modeling capabilities and machine data in the CL model building process. In addition to scanner effects, we study laser bandwidth tuning effects and the accuracy of corresponding model predictions by comparison against experimental data. The data demonstrate that the models predict well wafer CD variations resulting from laser BW tuning. We also find that using realistic spectral density distribution of the laser can provide more accurate results than the commonly assumed modified Lorentzian line shape.

**Keywords:** computational lithography, predictive model, GRAIL, OPC, verification, scanner tuning, laser bandwidth

## 1. INTRODUCTION

Computational lithography (CL) is becoming a fundamental cornerstone of advanced semiconductor processing technology. Besides well established model-based optical proximity correction (OPC) and full-chip OPC verification, new CL applications are emerging outside the traditional realm of electronic design automation (EDA), and are beginning to bridge the traditional boundaries between design, process development, and manufacturing. These new computational technologies include rigorous source-mask co-optimization (SMO), scanner specific layout verification, and model-based scanner tuning, which are becoming indispensable enablers of yield optimization throughout process development and manufacturing.

As these new applications aim at process window enhancement through model-based analysis or manipulation of the exposure tool, they pose more stringent requirements on modeling of the lithographic process than traditional CL applications related to model-based OPC (MBOPC). Whereas early MBOPC only required the model to predict CD or edge placement errors at the nominal process condition, at which the OPC model would be calibrated, current models must accurately predict patterning behavior over a range of dose and focus variations thus enabling process-window analysis. The MBOPC platform must be able to support full-chip simulation for effective and reliable scanner tuning of actual device layouts. [1]

The capability of full-chip CL models to accurately predict across a continuum of focus-exposure conditions has been established some time ago, and has been utilized e.g. in process-window aware OPC. [2,3] Also, capabilities of CL models to extrapolate and predict outside of optical conditions of the original model calibration has been demonstrated. [4] Such capability was historically required mostly in the context of early process development, when preliminary OPC models are needed for design rule exploration, while providing trustworthy prediction of patterning performance on a future scanner generation. A key requirement to model predictability with respect to extrapolation of optical parameters is separability between model components representing mask, scanner and resist, respectively. Model separability can only be achieved by accurate input of physical model components, and suitable calibration procedures, to avoid the coupling of optical or mask effects with the resist model during calibration. A separable model will allow extrapolation

beyond the original data sets, and towards new or detuned optical conditions by changing a corresponding physical parameter in the optical model, while keeping resist and mask model terms constant. Testing model separability by comparison of simulations from the extrapolated model against wafer data provides a sensitive test of model quality in general and is essential for qualification of a model for advanced applications.

Compared to extrapolating models in early process development, model-based scanner tuning will put qualitatively and quantitatively much more stringent requirements on CL models, as CD accuracies may be required to be in the nanometer or sub-nanometer range. While accurate physical models of scanner subsystems, such as the illuminator optics, can improve the overall model accuracy for OPC they are not the enablers for minimized edge-placement errors. However, these inputs are indispensable for scanner tuning and must represent all actuators or ‘knobs’ that are available for tool and process optimization.

In this paper we continue our assessment of various machine parameters that influence CL model quality, and demonstrate model prediction improvements by utilization of available scanner data or component models, which may be machine specific or machine-type specific. We then assess in-depth model sensitivity and quality with respect to effects of laser bandwidth variation. This part of the study is motivated by recent introduction of laser bandwidth tuning capabilities on Cymer lasers.[4] We provide a numerical test of pattern sensitivities with respect to laser bandwidth and a comparison against experimental data, comparing alternative methods of expressing finite laser bandwidth in the optical model. We also demonstrate that usage of actual laser spectrum provides better correlation with experimental bandwidth tuning sensitivities than the commonly used modified Lorentzian line shape assumption, which is in agreement with previous findings.[5] All simulation and modeling is performed on Brion Technologies’ Tachyon platform.

## 2. IMPACT OF SCANNER DATA ON OPTICAL MODELS

Here we follow up on a prior study [6] of the importance of scanner data in computational litho models, investigating scanner specific models for the ASML XT:1900i immersion exposure system. We derived a ranking from CD sensitivities induced by the various scanner parameters available in Tachyon optical models. All models are pure aerial image models using constant threshold and no resist model. We simulate CDs across a wide range of ~1300 test patterns that are similar to typical gauge patterns for OPC calibration purposes and are assumed to provide sufficient coverage of pattern geometry variability representative for logic type device patterns.

These gauges include several types of 1D and 2D patterns, i.e.: I) Line/Space through pitch; II) L/S with assist bars; III/IV) 2-bar patterns line or space CDs; V) end-of-line (EOL); VI) end-of-line ‘T’ shaped; and VII) a range of ‘generic’ 2D patterns. A comparison is then made between the baseline model CDs using a model without specific scanner data, and models which include specific machine parameters. Plots of the resulting CD differences may indicate a certain ‘sensitivity fingerprint’ of particular machine effects, and therefore help identify pattern types and their variabilities due to particular inputs in the model over the assumed range of or by variability in the input parameter.

The basic consideration is that inherent errors in the optical model will be partially compensated by the resist model when calibrating the full CL process model, or lead to residual fitting errors. In either case, the model quality will suffer. Compensation or masking of optical effects by resist terms will result in a less physical and less predictive model than when using realistic, physical parameters. The same applies for mask making effects and mask topography effects that arise from interaction of light with the edges of the finite depth mask absorber film stack. For comparison with the scanner effects we include mask topography, or m3d, effects here, modeled by an approximate numerical approach fast enough to enable full-chip model applications. We previously found that m3d effects can have significant impact on model predictability, but can also be rather effectively masked by resist model calibration. [6]

Finally, two different illumination settings are considered, both at 1.35NA and using X-Y polarization, a) a C-Quad illuminator with 20 degree pole angle and inner/outer sigma of 0.64/0.9; b) annular illumination with inner/outer sigma of 0.73/0.88. Individual machine data are tested for typical values of stage vibration MSD<sub>xy</sub> and MSD<sub>z</sub>, spec values for laser bandwidth, and design data for the Jones pupil of the projection lens. To assess the impact of realistic source map, compared with a top-hat illuminator profile, we consider both a measured source map from a particular machine, and a source profile derived from a database of specific DOE (diffractive optical element) characteristics and a physical model of the illuminator optics labeled as ‘GRAIL’. This predictive model will deliver a realistic, but idealized, source intensity

distribution without any need for in-situ metrology, measurement noise or residual imperfections of an actual exposure tool.

The results are plotted in Figure 1, ranked by the magnitude of their overall rms impact across all the gauge patterns. Besides the mask topography (m3d) model –comparing against Kirchhoff thin mask assumption-- we also show the effect of all scanner parameters combined, using GRAIL illuminator profile in this case. As discussed previously, illuminator characteristics are by far the dominant scanner contribution, and both measured source map and GRAIL show comparable effects, while the impact of the m3d mask model is even larger by the metrics employed here. [7] These observations are consistent with the previous findings that including realistic source maps and m3d modeling can clearly improve predictability and extrapolation power of a calibrated litho model, compared with top-hat illumination profiles or thin mask assumption.

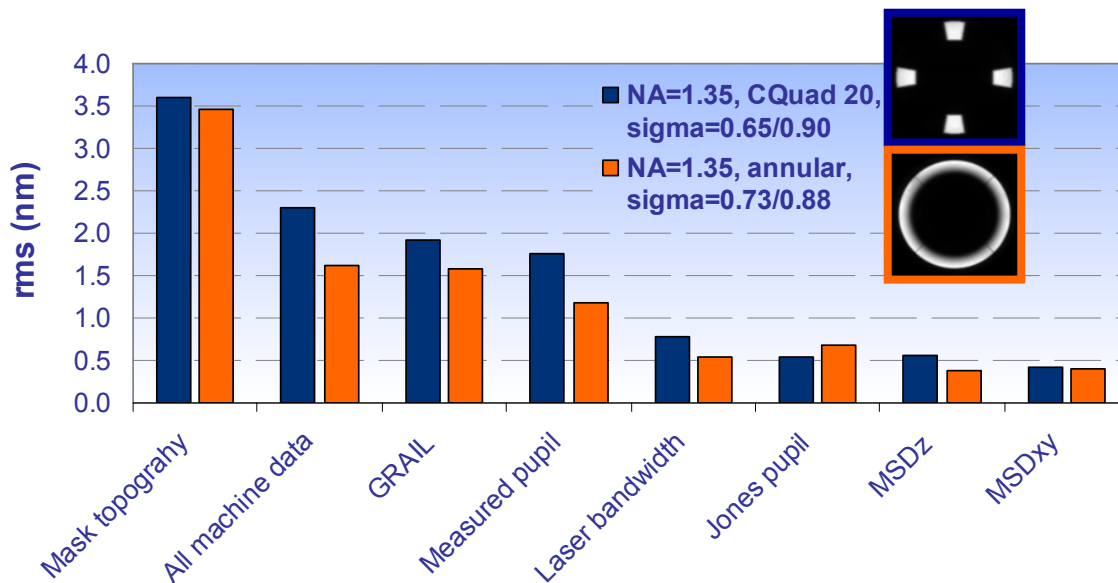


Figure 1: Ranking of physical model parameters by rms impact on aerial image CDs across set of OPC gauge patterns

However, there is no dominant second order scanner effect, as the model impact of MSD, laser bandwidth and Jones pupil are at similar levels, with minor differences between the two illumination modes. The magnitudes of these effects appear rather comparable to typical wafer metrology noise levels. However, it has been possible to demonstrate improvements in fitting accuracy of scanner-specific models through utilization of all available machine data in experiments where special attention was put on robustness of calibration gauges and extensive cleaning and filtering of input wafer data. [8]

To add to our prior observations, in Figure 2 we compare the currently accepted practice of using the in-situ measured illuminator source map as the only machine specific data with an alternative approach that uses the GRAIL predictive illuminator model, which would lend itself more suitably to possible scanner tuning applications, and using all available machine data. The experimental procedure and details have been previously described in Ref. [6]. In short, base models are generated by model calibration (fitting) at one process setting --here NA=1.15, annular illumination with sigma inner/outer=0.64/0.9 -- based on wafer CD data generated on an ASML XT:1700i scanner under multiple FEM dose and focus conditions. These are full CL models that comprise mask topography and effects due to the mask manufacturing process; the optical model describing illumination and projection optics; and an empirically-based resist model that captures blurring of the aerial image, and acid / base diffusion or other similar effects. Additional wafer CD data is generated after detuning the scanner to new optical conditions by offsets in NA and sigma settings, and this data is used to test model CD predictions of detuned models, which are generated from the calibrated base models by changing only the specific values of NA and sigma according to the new experimental settings. For the model using measured source map, the illuminator profile is also re-measured at the tuned conditions and imported into the corresponding models. With GRAIL, no scanner metrology is required to determine the source maps. There is no recalibration at the tuned

conditions, but a small dose offset on the order of 1% may be allowed in some cases to account for possible fluctuations between the wafer exposures under different conditions.

Figure 2 depicts the base fitting and tuned prediction rms between model and wafer CDs for the two modeling approaches under study. While the model fitting has been done across multiple focus and dose conditions to improve model robustness, the data shown here represents the nominal condition (NC) only, in order to reduce the influence of metrology noise on this comparison; the quality of wafer data is normally lowest at NC. There is only a minor difference in fitting rms between model A (measured source maps) and model B (GRAIL and advanced scanner parameters), potentially suggesting a small improvement by inclusion of additional scanner data. A more likely interpretation is that the actual differences between GRAL and source measurement –e.g. due to measurement noise and residual tool setup imperfections—are effectively compensated by the resist model.

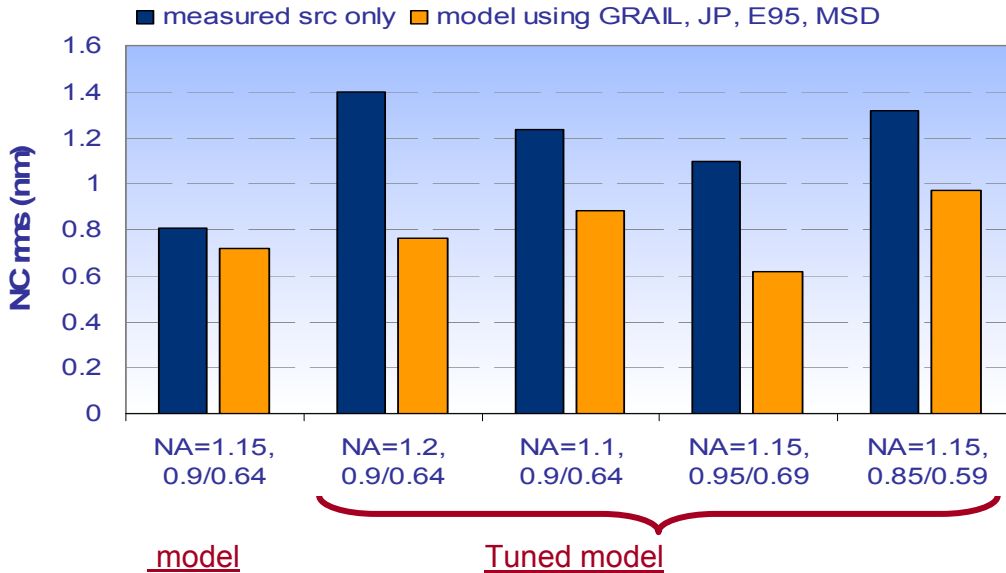


Figure 2: Improved model prediction through utilization of scanner data

On the other hand, interpretation of the model prediction results is very clear and unambiguous: there is significant improvement in model prediction for model B using all available scanner data. The prediction rms for model B is at a comparable level as the fitting rms of the base model, with some variation between conditions, corresponding mainly to variation in the noise level of the wafer data. As we previously found roughly comparable model prediction performance between GRAIL model and measured source maps, we attribute the noticeable improvement shown here mainly to including MSD, JP and laser bandwidth in the models here. We conclude that despite appearing almost negligible at first look at Fig.1, these scanner data apparently do have a clearly measurable combined net effect on model quality. From the small difference in fitting rms, we also conclude that it would be difficult to obtain the correct values for MSD and laser bandwidth from fitting generic image blur parameters during model calibration; accurate input of these effects for the experimental data set in question is required

### 3. DETAILS OF LASER BANDWIDTH EFFECTS AND TUNING

The results in Figure 1 above are slightly modified from our previously published results;[7] to use the E95 bandwidth values derived from the target bandwidth of current generation immersion lasers which are shipping in volume. This consideration as well as the new availability of active bandwidth stabilization and tuning on Cymer lasers motivated a more in-depth analysis of the impact of laser bandwidth and the need for including bandwidth information for CL modeling.

Obviously, the ranking of the importance of scanner parameters discussed above is directly dependent on the exact value considered to be typical for the various scanner parameters. As mentioned, we adjusted the ‘nominal’ value of E95 laser

bandwidth to a new value of 0.3 $\mu$ m in Fig.1. This did not change our ranking of machine parameters compared with prior results. However, Figure 3 illustrates the dependence of the rms metrics employed here on the actual value of laser bandwidth. It indicates that at a slightly higher E95 value around 0.35-0.4 $\mu$ m, the impact of laser bandwidth –compared against a generic, monochromatic model— would appear to be of similar magnitude to the impact of realistic source maps compared against generic top hat illuminator models. This may not be a completely straightforward comparison due to the higher complexity and more degrees of freedom of illuminator pupil effects, but it confirms the need to pay attention to laser bandwidth effects, in particular for the more aggressive off-axis C-quad illuminator profile.

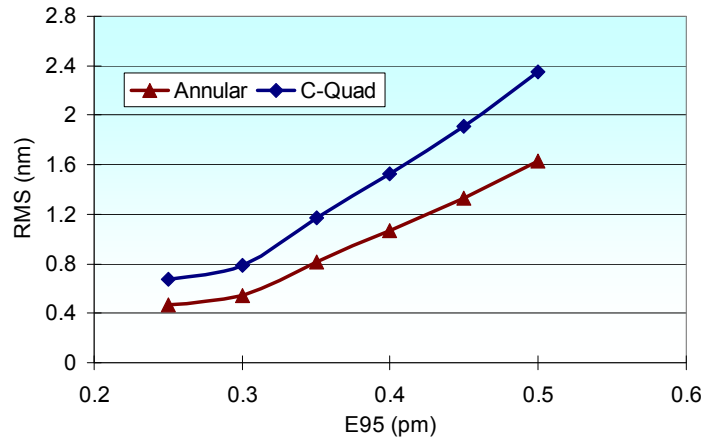


Figure 3: Increasing impact of laser bandwidth with increasing E95. The same RMS metrics is used as in Fig. 1.

Fig. 4 plots the individual CD differences from generic baseline models. The blue and red curves correspond to the data points in Fig. 3 at 0.25 $\mu$ m and 0.5 $\mu$ m, respectively. The CD deltas are plotted against gauge number, where the gauges are sorted into test pattern groups as indicated in the figure and described above.

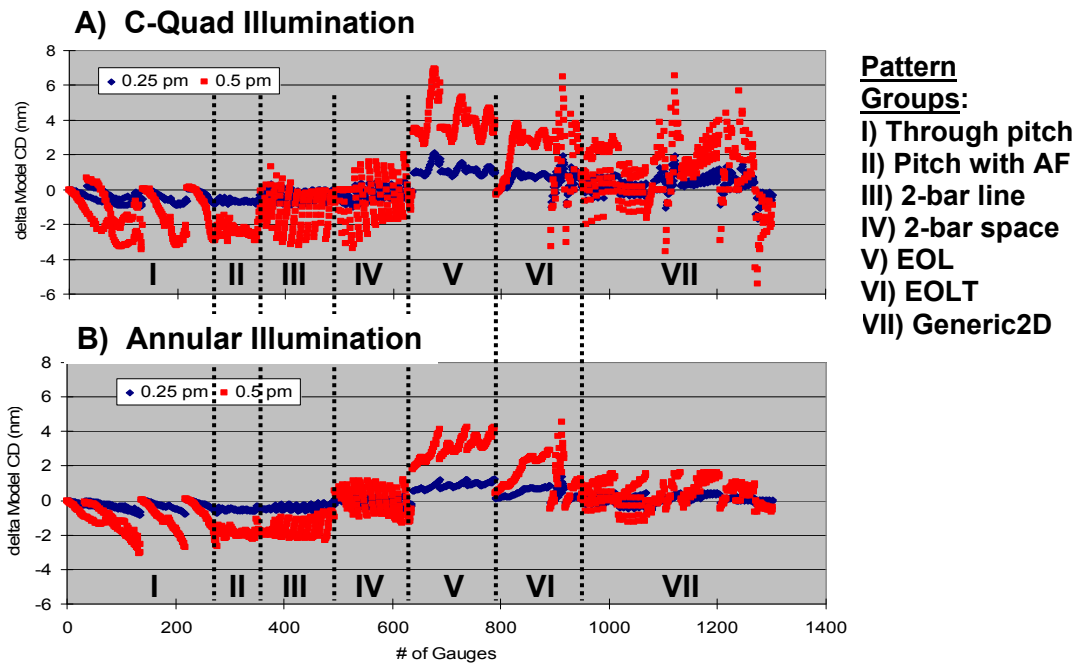


Figure 4: CD change induced by laser bandwidth models vs generic baseline models across 1300 test patterns.

Between the two different illumination modes not only the overall magnitude of the laser BW sensitivity differs, but also its ‘fingerprint’ across the different test patterns and pattern types displays considerable differences. We note in particular the large variations, i.e. sensitivity to BW changes for some of the ‘generic 2D’ gauges in case of the C-quad models. The rms differences between annular and c-quad illumination seen in Fig.4 are mostly related to larger differences for the asymmetric 2-bar, EOL and generic 2D patterns. This might suggest a complex interaction between illuminator shapes, pattern shapes and focus blur through finite laser bandwidth. However, a more detailed investigation of this is outside the scope of the current paper.

In the following, we study the effects of laser BW tuning and the accuracy of our CL model by comparison against experimental data. We are trying to answer the question if the model can predict wafer CD variations resulting from laser BW tuning, which adds a new dimension to the previously discussed model extrapolation along NA and sigma adjustments. We also compare two alternative representations of the finite laser bandwidth, which have been recently discussed in literature.

All laser bandwidth modeling referred to in this paper so far used the well known modified Lorentzian (ML) line shape [9], which is available as a built-in option on the Tachyon model platform. In most cases, both the full width at half maximum (FWHM) and E95 values of the laser are known, allowing the order  $n$  of the ML form to be adjusted such that both bandwidth metrics are met by the line shape. Typically this leads to a value of  $n \sim 3-3.5$ , which produces a steeper roll-off than the Lorentzian line shape with  $n=2$ , but compared with an actual laser spectrum the tails of the ML spectral distribution will still be wider. [9] As alternative, we consider the input of a measured laser spectrum obtained at the factory by Cymer, with a wavelength range covering approximately  $2.2 \times E95$  centered around the peak intensity. This measured spectrum is re-sampled within our simulation tool at a certain granularity to produce a realistic laser spectrum approximation (LSA), similar to the approach discussed in Ref. [10]. As has been shown previously, we see that the ML distribution covering a wavelength range of  $2.2 \times E95$  results in higher RMS errors than the LSA with covering comparable wavelength range. In this case, re-sampling the ML form over a smaller range ( $1 \times E95$ ) can be used to minimize the RMS errors at best focus for this bandwidth condition.

The experiments were performed on the same XT:1700i scanner and same exposure conditions as discussed for base model calibration in the NA-sigma model tuning study in Fig.2 above, but rather than tuning a scanner adjustment, the particular XLA 360 laser was retrofitted with a prototype bandwidth tuning module. This allowed adjustment of the E95 setpoint over a range of 4 FEM wafer exposures with E95 bandwidth values of 0.24, 0.28, 0.4, and 0.5 pm, respectively. NA and sigma were kept at 1.15NA and  $\sigma_{inner/outer}=0.64/0.9$  for annular illumination.

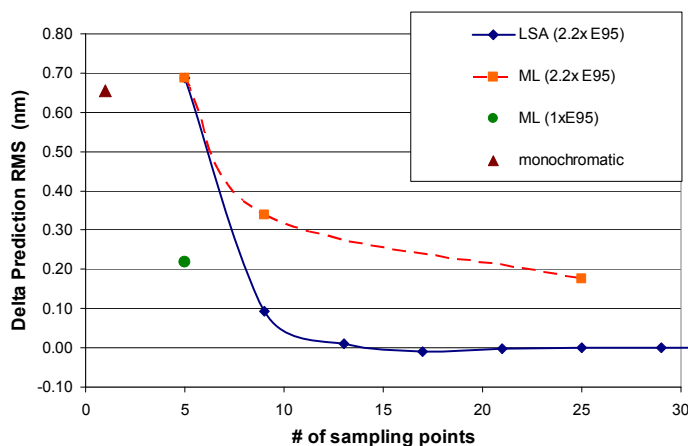


Figure 5: Convergence of model results with varying sampling rate of the laser spectrum approximation (LSA) and comparison with modified Lorentzian (ML) approximation

For assessment of model quality, we will initially follow the same principle as before, i.e. do model calibration at one condition, then compare extrapolated –after change of laser BW in the model–, predicted model CDs against wafer data generated at the corresponding tuned condition. In order to strike a balance between model calculation time and inherent accuracy, we first check the convergence of the tuned model prediction with the re-sampling rate of the laser spectrum internal to the simulation engine. For this quick test, an initial model is calibrated against wafer data from the 0.24pm condition, using the complete available laser spectrum, and a number of detuned models are then generated with E95=0.5pm but different # of sampling points of the laser spectral density distribution.

Within the scope of this paper we limit ourselves to a regularly spaced sampling centered around the peak intensity, and covering the complete range of the baseline spectrum (2.2x $E_{95}$ ). More efficient spectrum sampling schemes are likely possible. Within this constraint, the convergence of model CD predictions towards the baseline case using the full LSA with 65 points is plotted in Figure 5 as CD rms difference over the set of calibration gauge patterns used in the experimental comparison below. These were limited to 1D line/space patterns –through pitch at various drawn line widths– in order to reduce the influence of metrology noise which is significantly larger for 2D patterns such as line ends. From Fig. 5 we conclude that a total number of close to 20 sampling points provides a sufficiently accurate LSA, in good general agreement with Ref. [10,11]. For reference, Figure 5 also indicates the CD rms difference between the full LSA and a monochromatic model without BW information, and a ML model with corresponding bandwidth, and covering the same wavelength range (2.2x $E_{95}$ ) as the experimental spectrum. The order of the ML is fitted to match both FWHM and E95 of the LSA. The corresponding rms data show a similar trend with sampling rate as the LSA data, and a net offset from the LSA reference. Finally, we also show a single data point for the same ML sampled with 5 points only, but covering only a range of 1x $E_{95}$  around the center wavelength, to illustrate the possible tradeoffs between sampling rate and wavelength range. For the remainder of this paper a 21-point representation of the LSA is used. Furthermore, all models use m3d, GRAIL-predicted illuminator shape, design Jones pupil data, and actual MSD numbers from the scanner.

A first result of model extrapolation under laser bandwidth tuning is shown in Figure 6. Two cases are considered to provide a check for self consistency of the observed effects. On the left hand side are results from fitting base models at the lowest BW condition and extrapolating towards the larger bandwidth settings, while on the right hand side the extrapolation proceeds in the opposite direction starting from models calibrated against wafer data from the E95=0.5pm case. All models and data plotted here are limited to nominal focus and dose settings only, to exclude any possible influence of elevated metrology noise from off-PW conditions.

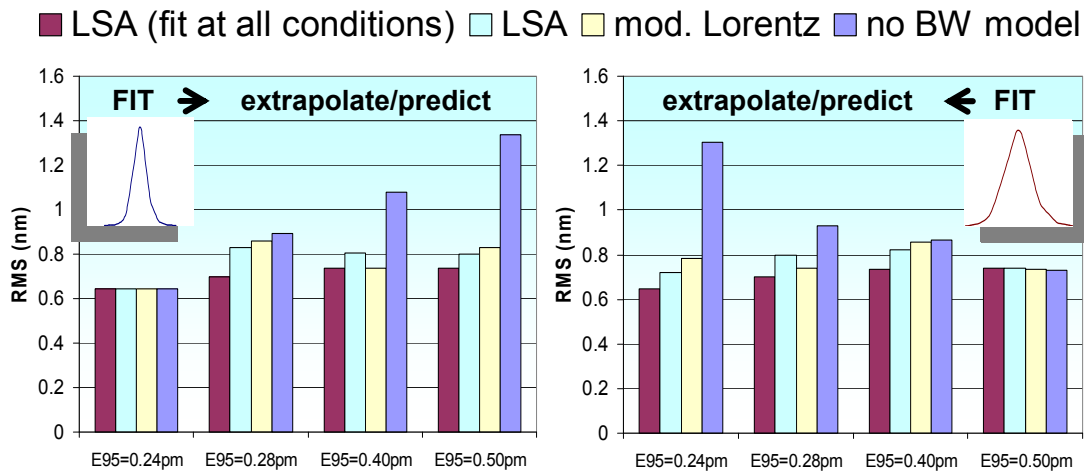


Figure 6: Model separability and prediction test under laser bandwidth tuning. Nominal PW condition data.

Both plots in Fig. 6 show two reference data sets. The first reference data set is obtained from comparing wafer data against models not using any laser BW information. Obviously there is no laser bandwidth tuning in the model, i.e.

the exact same model is compared against wafer CD data for all 4 conditions. This data set indicates the net effect of laser tuning on the wafer data, and it shows continuous increase with detuning from the calibration condition in either tuning direction with very similar magnitude.

The second reference data set, labeled “LSA (fit at all conditions)” shows the calibration fitting rms for all 4 BW settings. At the two intermediate conditions, the fitting rms is only plotted for the LSA model; however, as clearly shown at 0.24pm and 0.5pm, there are no significant differences in fitting rms between the 3 different model types. This second reference data set essentially indicates the best rms between model CDs and wafer data and shows very minor variation across all 4 bandwidth conditions. The fact that no significant differences occur between fitting rms of the different model types indicates that differences between the aerial image characteristics between the three optical models are completely compensated and masked by the empirical resist model during the calibration.

Clearly, coupling bandwidth effects into the resist model makes the model less predictive; in the trivial case of not modeling laser BW at all, the model can not predict the real effects of BW tuning on wafer CDs. Including laser BW information in the model –here by using either a ML or LSA model—clearly provides good prediction capabilities and brings the rms at extrapolated conditions close to fitting rms. However, in this test we don’t recognize a systematic difference between the two bandwidth models under comparison.

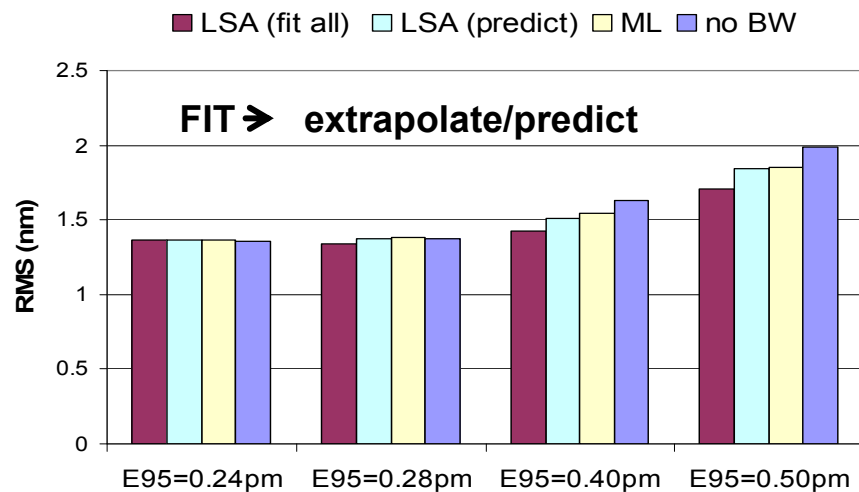


Figure 7: Model separability and prediction test under laser bandwidth tuning, considering FEM models across 4 defocus conditions.

In Figure 7 we show an equivalent plot of fitting and prediction data, where fitting is done against wafer data over multiple defocus conditions and prediction rms values are calculated for the same FEM conditions. The overall rms level is higher than in Fig 6, which makes the systematic detuning effect a little less obvious, but the general observations remain the same: no difference in fitting rms between model types, and improved prediction with laser BW models. On the other hand, fitting across multiple FEM conditions is expected to make the resulting models inherently more robust, while the differences between LSA and ML models are expected to be larger at off-focus conditions.[10] Fig. 7 does show a more systematic behavior between ML and LSA models, and with some good will one may argue a very small advantage of the LSA model input.

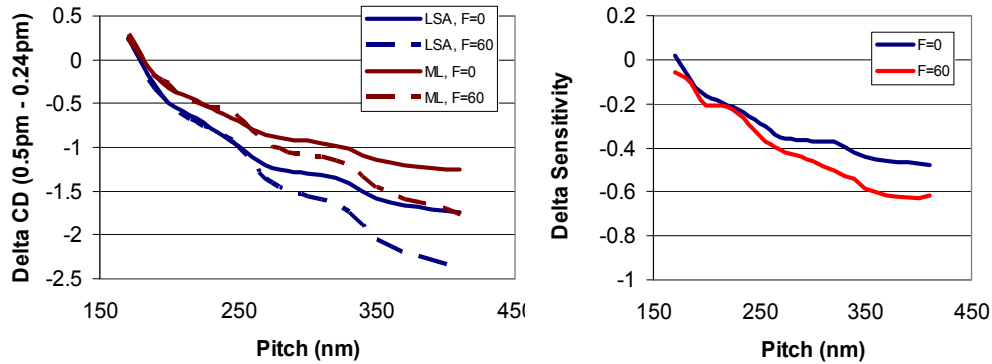


Figure 8: Simulated pitch and defocus dependency of BW sensitivities, i.e. CD change induced by bandwidth tuning (left) and differences between model types.

For further insight, in Fig. 8 we plot the model CD difference induced by laser bandwidth tuning from 0.24pm to 0.5pm for one of the through pitch L/S patterns, here with drawn CD of 80nm. On the left hand side, we plot CD differences through pitch for 2 defocus conditions and the two bandwidth models. The right hand side shows the sensitivity difference between the two laser models, i.e. the difference between the Delta\_CD numbers from the left hand plot. As in previously published data, Fig. 8 shows that a) through-pitch isolated features tend to be more sensitive to laser BW effects overall, as well to the differences between ML and LSA modeling, and b) the latter differences appear somewhat enhanced at defocus conditions.

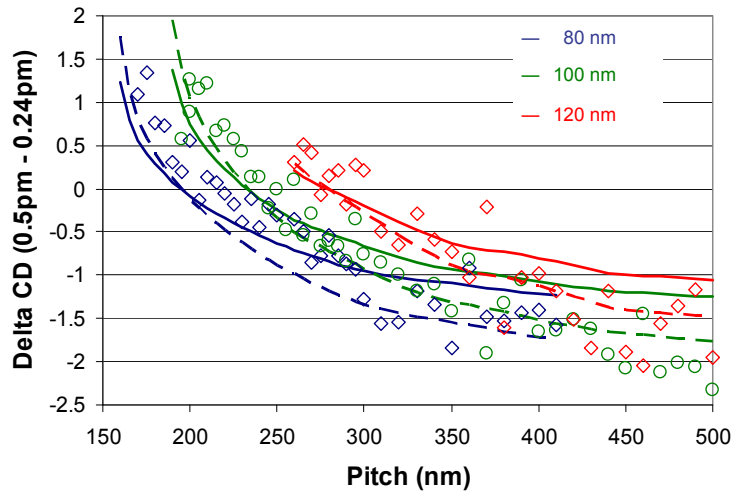


Figure 9: Pitch and defocus dependency of experimental and model CD changes induced by BW tuning. Dashed line: LSA model; solid line: ML model; drawn line widths are 80, 100, 120nm.

Consequently, as the gauge patterns used in model calibration and prediction span across dense and semi-isolated pitches, overall rms will not be the best metrics to judge differences between the ML and LSA modeling approaches, and it is generally unable to predict patterning effects on individual features. In Figure 9 we compare directly the modeled CD sensitivities, i.e. CD differences induced by laser BW detuning, between LSA model (dashed lines), ML model (solid lines) and wafer data for 3 different drawn line widths through pitch. The general trend of the wafer data is in agreement with the model predictions, and the LSA model appears somewhat closer to

the experimental data points. On the other hand, the differences between the two models appear to be comparable to the experimental uncertainty.

For a clearer picture and quantitative assessment we consider the correlation between experimental and modeled tuning sensitivities –now expressed as CD change over laser bandwidth change in nm/pm. Fig. 10 plots the simulated data points against experimental data points for all test patterns within the calibration/prediction gauge data set. The figure also shows a linear fit of the data points, where a slope of 1 would indicate perfect agreement between experiment and model. There is some residual systematic error for both model types, but clearly the LSA model provides a more accurate representation of the wafer data than the ML model in this analysis.

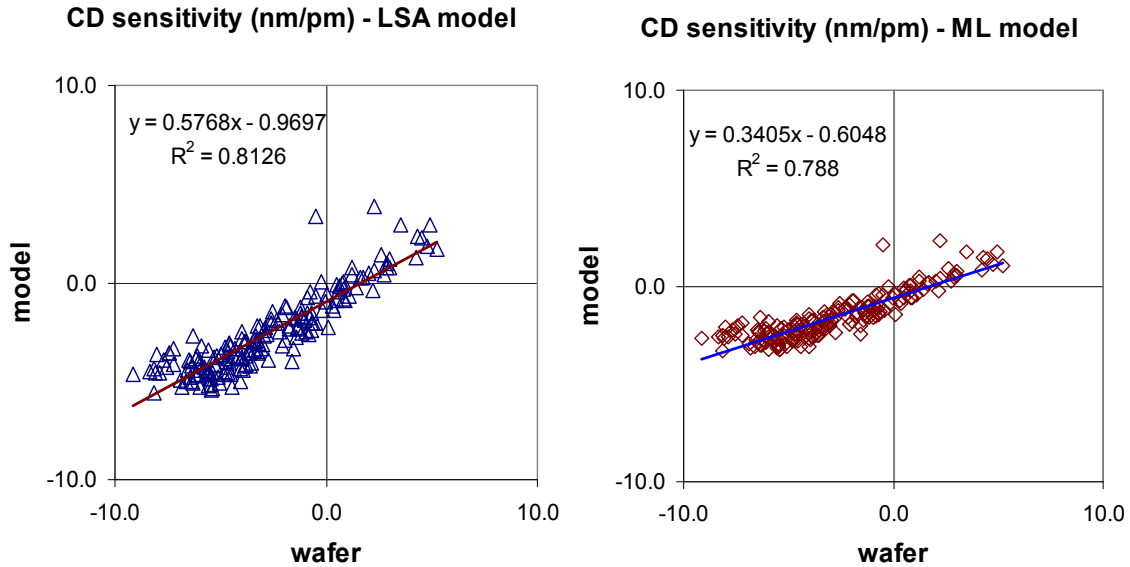


Figure 10: Correlation between experimental and modeled CD sensitivities of to bandwidth tuning

#### 4. SUMMARY & CONCLUSION

We study the impact of real scanner data and laser bandwidth data on the accuracy and predictability of full-chip computational lithography (CL) models. While illuminator pupil effects are generally recognized as the dominant influence on CL model accuracy, we show that other machine effects such as MSD, Jones pupil, and finite laser bandwidth all contribute to a measurable net effect on model accuracy. We demonstrate by verification against wafer data that including realistic machine data in model generation improves model quality by improving the separability of optical and resist model components. Improved model predictability allows more accurate simulation of patterning results at extrapolated optical process settings that are detuned from the specific condition for which the model was calibrated.

Furthermore, we study in some detail the effects of finite laser bandwidth, and present an experimental study of bandwidth tuning effects, together with an assessment of current modeling capabilities to predict the BW related CD changes. The tuning capabilities of current state-of-the-art ArF light sources provides an effective actuator to influence optical proximity effects on printed patterns, and accurate models are required to reliably simulate these effects in advanced CL applications. The data show that our current modeling capabilities provide a reliable representation of bandwidth effects. The results also confirm noticeable differences between an idealized representation of the laser spectrum by a modified Lorentzian line shape and a realistic 'laser spectrum

approximation' derived from experimental data. We analyze the data in terms of BW tuning sensitivity across a range of test patterns, and demonstrate significantly improved model accuracy when using realistic spectral data.

In conclusion, we demonstrate significant improvements of accuracy and predictability of full chip CL models by including realistic optical data from the laser and scanner. The added accuracy in predicting not only patterning, but also tuning effects is expected to meet the needs of emerging new CL applications.

\*stefan.hunsche@brion.com; phone 1-408-653-1512; fax 1-408-653-1501; www.brion.com

## ACKNOWLEDGEMENT

The authors wish to thank Peng Liu of Brion for additional analysis and useful discussions.

## REFERENCES

- [1] C.Y. Shih, R.C. Peng, T.C. Chien, *et al.*, "Model-based scanner tuning in a manufacturing environment", Proc. SPIE 7274 (2008).
- [2] Luoqi Chen, Yu Cao, Hua-yu Liu, Wenjin Shao, Mu Feng, and Jun Ye, "Predictive focus exposure modeling (FEM) for full-chip lithography", Proc. SPIE 6154 (2006).
- [3] Mark Terry, Gary Zhang, George Lu, *et al.*, "Process window and interlayer aware OPC for the 32-nm node", Proc. SPIE 6520 (2007).
- [4] Vladimir Fleurov, Slava Rokitski, Robert Bergstedt, *et al.*, "XLR 600i: Recirculating Ring ArF Light Source for Double Patterning Immersion Lithography", Proc. SPIE 6924 (2008).
- [5] Ivan Lalovic, Oleg Kritsun, Joseph Bendik, *et al.*, "Fast and accurate laser bandwidth modeling of optical proximity effects", Proc. SPIE 6730 (2007).
- [6] Hua-Yu Liu, Qian Zhao, J. Fung Chen, *et al.*, "Separable OPC models for computational lithography", Proc. SPIE 7028 (2008).
- [7] Stefan Hunsche, Xu Xie, Qian Zhao, *et al.*, "Scanner-specific separable models for computational lithography", Proc. SPIE 7122 (2008).
- [8] Peter Nikolsky, Tjitte Nooitgedagt, Paul van Adrichem, *et al.*, "OPC cycle time reduction and accuracy improvement", Proc. SPIE 7122 (2008).
- [9] Timothy Brunner, Daniel Corliss, Shahid Butt, *et al.*, "Laser bandwidth and other sources of focus blur in lithography", J. Microlith., Microfab., Microsyst. 5(4), 2006.
- [10] Ivan Lalovic, Oleg Kritsun, Joseph Bendik, *et al.*, "Defining a physically accurate laser bandwidth input for optical proximity correction (OPC) and modeling", Proc. SPIE 7122 (2008).
- [11] Peter De Bisschop, Ivan Lalovic, Fedor Trintchouk, "Laser bandwidth and other sources of focus blur in lithography", J. Microlith., Microfab., Microsyst. 7(3), 2008.